Laboratory measurements of artificial rain impinging on slick-free and slick-covered water surfaces

Nicole Braun, Martin Gade, and Philipp A. Lange

Institute of Oceanography, University of Hamburg, Hamburg, Germany

Abstract. Laboratory measurements with artificial rain were carried out in the wind-wave tank of the University of Hamburg, in order to gain better understanding of the radar backscattering from a slick-free and slick-covered water surface, particularly when it is agitated by strong rain. We used a coherent 9.8 GHz (X band) scatterometer at different polarisations and at an incidence angle of 28 degrees, a resistance-type wire gauge, and a two-dimensional laser slope gauge. A water surface area of 2.3 m^2 was agitated by strong artificial rain with a rain rate of 160 mm h^{-1} and rain drops of 2.9 mm diameter. The wind-speed range used in the present investigation was between 2 and 10 m s^{-1}. A monomolecular surface film was produced by deploying oleyl alcohol on the water surface. The results of the analyses of the measured radar Doppler spectra and wave amplitude and slope spectra are presented. We show that while the wind-induced surface roughness is strongly reduced in the presence of the slick, at a high rain rate (of 160 mm h^{-1}) the surface slick less strongly affects the rain-induced increase of the surface roughness (i.e., the generation of crowns, cavities, stalks, ring waves, and secondary drops).

1 Introduction

Radar signatures of rain events are often observed on synthetic aperture radar (SAR) images of the ocean surface because rain drops impinging on the sea surface change the surface roughness in at least two ways: (1) roughness is increased because the rain drops generate ring waves, crowns, cavities, and stalks, and (2) roughness is decreased because they generate turbulence in the upper water layer which in turn dampens the wind generated water waves. Moreover, oceanic surface films (be they of biogenic or anthropogenic origin) strongly influence the backscattered radar power (σ_{rel}) by damping the small-scale surface roughness, which is responsible for the radar backscattering at oblique incidence angles (between 20 and

75°, so-called Bragg waves). Figure 1 shows subsections of three SAR images of the Atlantic Ocean, north of the Azores, acquired on April 12th, 1994, at 0721 UTC by the Spaceborne Imaging Radar C/X Band SAR (SIR-C/X-SAR) at L-, C-, and X-band (from left to right), VV polarisation. The diagonal dark narrow line visible on the three images is caused by freshly spilled mineral oil, and the irregular bright spot in the image centre is caused by strong rain. This example shows the different imaging of the two counteracting phenomena (surface film and strong rain) at the different radar bands: the contrast is highest at X-band, and it is lowest at L-band. A more detailed analysis of the described phenomena can be found in Melsheimer et al. (1998) and Braun (1998), respectively.

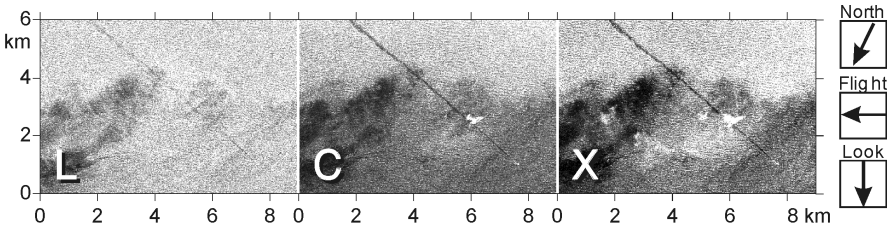

Fig. 1. Subsections of three synthetic aperture radar (SAR) images of the Atlantic Ocean, north of the Azores, acquired on April 12th, 1994, at 0721 UTC by the Spaceborne Imaging Radar C-/X-Band SAR (SIR-C/X-SAR) at L-, C-, and X-band (from left to right), VV polarisation. The diagonal dark narrow line is caused by freshly spilled mineral oil, whereas the irregular bright spot in the image centre is caused by strong rain

Braun et al. (2002) presented results from laboratory studies of the influence of artificial rain on the measured water surface elevation and slope, and, moreover, on the radar backscattering from a rain- and wind-roughened slick-free water surface. In order to complement their findings, we performed a second measurement series, where we investigated the influence of artificial rain on a slick-covered water surface. The aim of these studies was to improve the classification of signatures visible on SAR images. In particular, for an effective surface film detection the influence of rain on the visibility of oceanic surface films has to be known. *Vice versa*, if spaceborne radar data is used for the estimation of rain rates (as proposed by Melsheimer et al. (1998)), one has to know how surface films affect the radar signal of (strong) rain events over the ocean surface. First results of our studies are presented herein.

2 Instrumentation

The wind wave tank of the University of Hamburg is 26 m long and 1 m wide. It is filled with fresh water with a mean water depth of 0.5 m. The wind-tunnel height is 1 m, and the effective (maximum) fetch is 19 m. All measurements reported herein were performed at a fetch of 14.5 m and at wind speeds between 2 and 10 m s^{-1} generated by a radial blower. In the measurement and rain area, the metallic plates of the tank's roof were removed and, on the leeward side, replaced by Styrofoam panels to ensure the unattenuated transmission of the microwaves (Figure 2). At the windward side of the rain area plates of microwave absorbing material were vertically mounted in the direction of the specular-reflected radar beams.

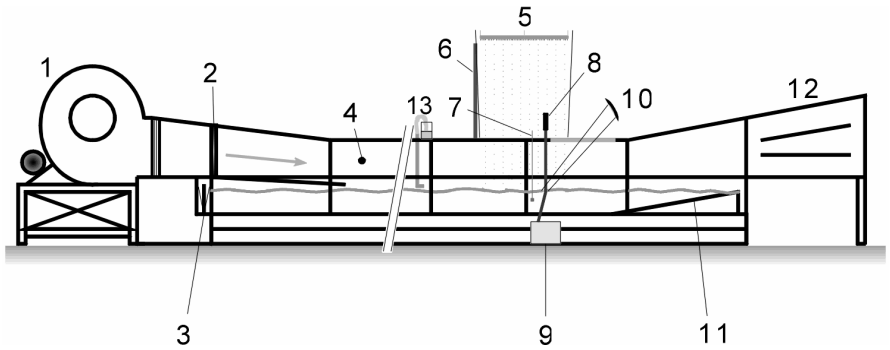

Fig. 2. Schematic side view of the wind-wave tank. 1: blower, 2: honeycomb, 3: wave flap, 4: anemometer, 5: rain generator, 6: radar absorber plates, 7: wire, 8: laser, 9: laser optics, 10: X band antennae, 11: beach and overflow baffle, 12: diffusor, 13: slick deployment.

The rain generator consists of six interconnected tubs (each 0.8 m long, 0.6 m wide, and 0.3 m high) which are mounted in an aluminum frame at a height of 4.5 m above the water surface. Approximately 2500 hypodermic needles are inserted in a triangular pattern with a distance of 3 cm into the bottoms of the tubs. The total area covered by the artificial rain is 2.3 m x 1 m. The diameter of the rain drops in our investigation was 2.9 mm and they attained an impact velocity of 8.1 m s^{-1} which is 85 % of their terminal velocity (Laws 1941). Monomolecular surface films were produced by deploying oleyl alcohol (OLA) dissolved in ethanol (75 mMol L^{-1}) on the water surface at a fetch of 5.5 m by using a pipette that was fixed a few millimetres above the water surface. The drops touched the water surface, thus allowing for optimum spreading of the monolayer without significant losses to the bulk.

The radar measurements were performed with separate upwind looking radar antennae for transmission and reception. We used a coherent continuous wave (CW) 9.8 GHz (X-band) scatterometer operating at a fixed incidence angle of 28°. The X-band microwave beam was focused on the water surface by means of a bistatic parabolic reflector construction mounted on a metal frame. The dimensions of the radar footprint on the water surface were 15 cm x 12 cm (range x azimuth). Wave heights were measured using a resistance-type wire wave gauge with a 0.075 mm diameter tungsten wire whose penetration point into the water was located at a distance of 22 cm laterally from the radar footprint (i.e., at the same fetch). Wave slopes were measured using a laser slope gauge whose footprint was at the centre of the radar footprint. The frequency resolution of the wire gauge is 30 Hz and of the laser slope gauge better than 100 Hz. The reference wind speed was measured at the wind entrance 65 cm above the mean water surface level using a propeller-type anemometer (Figure 2).

3. Results and Discussion

Various data sets were obtained by using the different sensors; however, in this paper we concentrate on results from measurements with the laser slope gauge as well as with the X-band scatterometer operating at co- (VV) and cross-polarisation (HV). In order to gain insight into the specific damping behaviour of OLA in the presence of rain, we calculated the normalised orientation ratio, NOR, which we define as

$$NOR(f) = \frac{S_y(f) - S_x(f)}{S_x(f)} \tag{1}$$

where $S_y(f)$ and $S_x(f)$ are the along-wind and crosswind wave-slope spectra, respectively. High values of the NOR denote a strong orientation of the wave field in the along-tank direction.

Some results obtained at different wind speeds are shown in Figures 3 and 4 for slick-free and slick-covered water surfaces, respectively. In both figures the NOR in the upper row were obtained without rain (rain rate 0 mm h^{-1}), and the NOR in the lower row were obtained at a rain rate of 160 mm h^{-1}. The columns denote different wind speeds (3, 5, 7, and 9 m s^{-1}, from left to right).

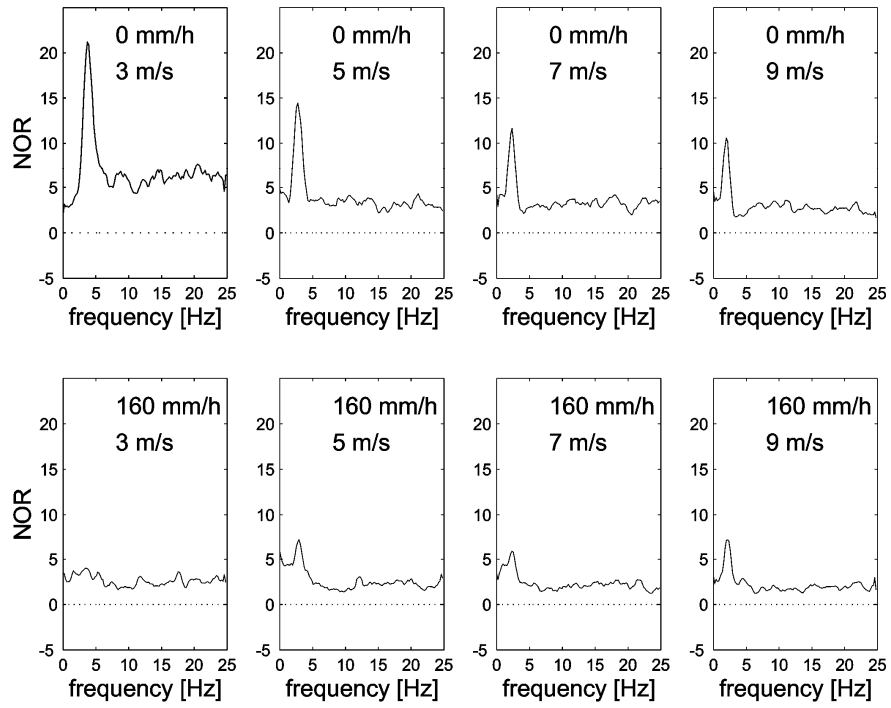

Fig. 1. Frequency dependence of the normalised orientation ratio, NOR (see (1)), measured with the two-dimensional laser slope gauge at different wind speeds (columns) without rain (upper row) and with rain at a rain rate of R=160 mm h^{-1} (lower row). The water surface was not covered with any slick.

In Figure 3 it is demonstrated how the strong rain decreases the effect of strong wave orientation, particularly at the frequency of the dominant wind wave: for each wind speed a sharp maximum of the NOR was observed without wind (upper row in Figure 3), but only a weak maximum was observed in the presence of strong rain (lower row in Figure 3). Even at high wind speeds (9 m s^{-1}) and at a rain rate of 160 mm h^{-1} the orientation of the wave field along the wind direction is still reduced.

The results shown in Figure 4 were obtained when the water surface was covered by an OLA slick. At 3 m s^{-1} (leftmost column), which is below the threshold wind speed for the first excitation of wind waves on a slick-covered water surface, only slight differences are caused by the rain (Figures 4a and e). However, at 5 m s^{-1} (Figures 4b and f) we measured strong differences: whereas a pronounced orientation of the wave field is observed from the maximum in Figure 4b (corresponding to the frequency of the dominant wave field), a less pronounced maximum was measured

when the water surface was agitated by rain (Figure 4f). The (non-oriented) ring waves, which are generated by the rain, cause a strong reduction of the NOR in the frequency range between 3 and 12 Hz (which is the characteristic frequency range of the ring-wave spectrum, see Bliven et al. (1997)).

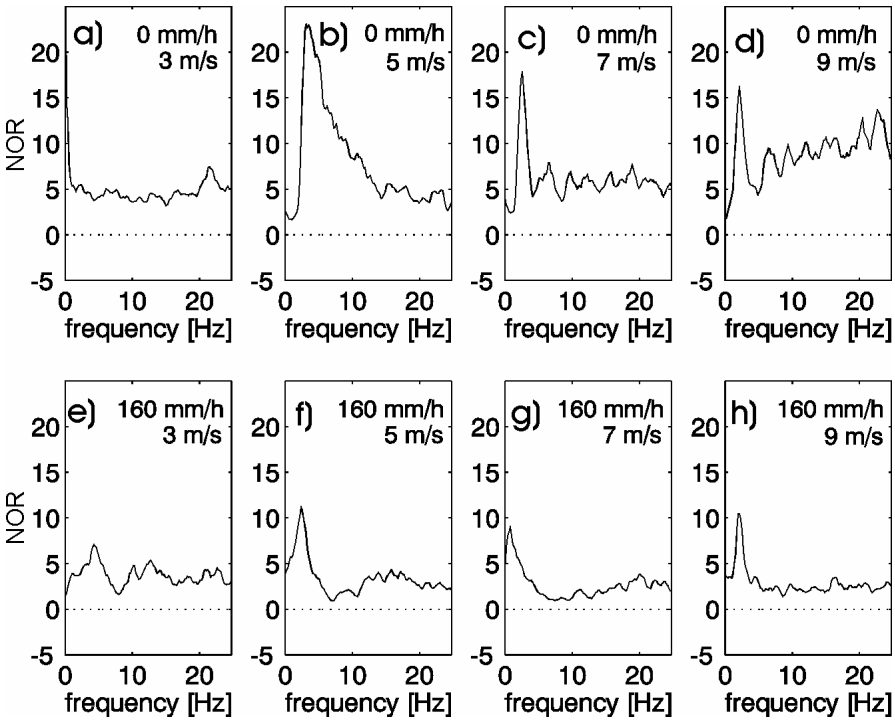

Fig. 2. Frequency dependence of the normalised orientation ratio, NOR (see (1)), measured with the two-dimensional laser slope gauge at different wind speeds (columns) without rain (upper row) and with rain at a rain rate of R = 160 mm h^{-1} (lower row). The water surface was covered with oleyl alcohol

At 7 m s^{-1} (Figures 4c and g) we measured a rain-induced decrease in the NOR also at higher frequencies (i.e., up to 25 Hz, compare Figure 4g). On the one hand, the high-frequency part of the wave-slope spectrum is strongly damped by the slick, particularly, those waves which are travelling in crosswind direction (and which are not directly generated by the wind). On the other hand, the high-frequency part of the ring-wave spectrum causes an additional reduction of the NOR at higher frequencies. Thus, the observed effect is caused by the two counteracting effects de-

scribed above (wave damping by the slicks and wave generation by the rain drops).

At 9 m s^{-1} (Figures 4d and h), again, we measured a reduction of the NOR in the presence of rain in the entire frequency range. However, we can infer from the sharp maximum in Figure 4h at about 2 Hz that at high wind speeds the wind-generated part of the slope-spectrum dominates over the rain-induced part only at low frequencies. The entire wind-wave spectrum is, therefore, more oriented than in the absence of any slick (cf. Figure 3).

Radar Doppler spectra measured at co-polarisation (VV-pol.) and at cross-polarisation (HV-pol.) are shown in Figures 5 and 6, respectively. In each figure the solid curves denote Doppler spectra acquired at a rain rate of 160 mm/h, and the dashed curves correspond to Doppler spectra acquired without rain. During the measurements the water surface was covered with a monomolecular OLA slick.

The Doppler spectra measured at VV-polarization, without rain (dashed curves in Figure 5), show that no X-band Bragg waves are generated at 2 and 4 m s^{-1} (Figures 5b, c). Moreover, at moderate wind speeds (6 and 8 m s^{-1}; Figures 5d, e) the existence of bound and freely propagating Bragg waves can be delineated from the different locations of the narrow spectral maximum (for details see Gade et al. (1998)).

The solid curves in Figure 5 (160 mm h^{-1} rain rate) show that the rain-generated ring waves are the main scatterers at wind speeds up to 8 m s^{-1}. It was already shown by Braun et al. (2002) that the occurrence of two peaks in the Doppler spectra (measured at co-polarisation) is caused by ring waves propagating towards and away from the radar antennae. These ring waves cause two separated peaks with an overall (mean) Doppler shift due to the wind-dependent surface drift.

At 10 m s^{-1}, the slicks are dispersed in both cases (wind only and wind plus rain). Thus, the Doppler spectra at co-polarisation measured with and without rain are similar and only a slight influence of the slick coverage is visible.

The Doppler spectra measured at HV-polarisation, without rain (dashed curves in Figure 6), show that no radar backscattering from a slick-covered water surface was measured up to wind speed of about 4 m s^{-1}. Moreover, at 6-8 m s^{-1} only a very weak backscattered signal was measured. At 10 m s^{-1}, where the surface film has already started to disperse, a significant radar Doppler signal was measured.

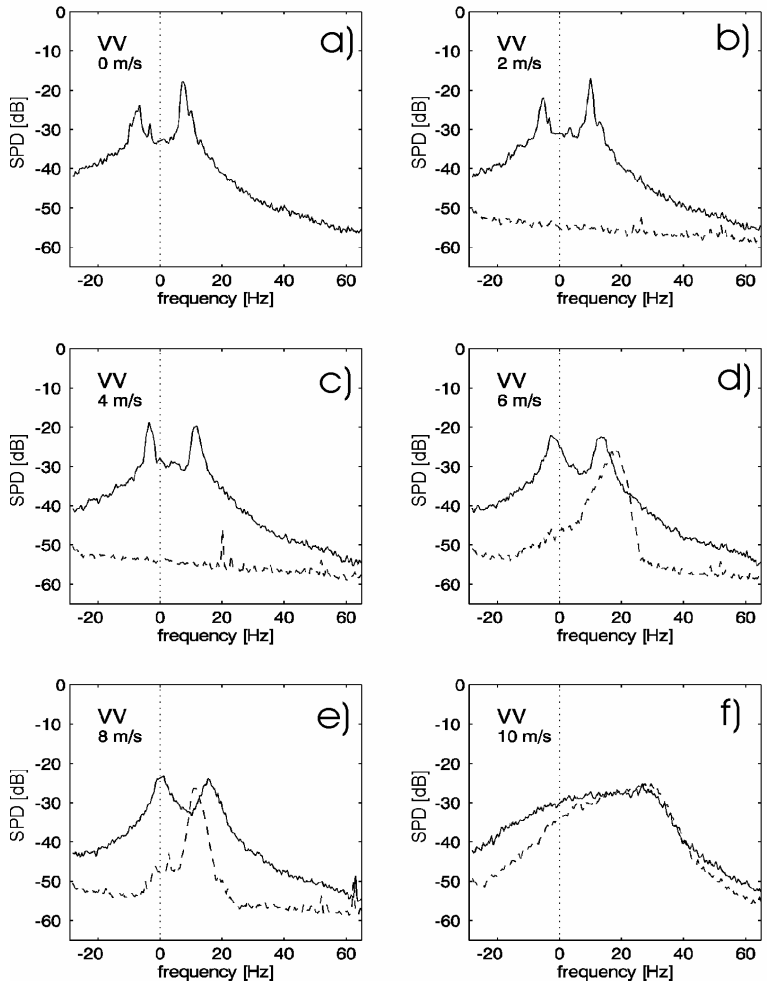

Fig. 5. Radar Doppler spectra measured at vertical polarizations (VV) and different wind speeds (0, 2, 4, 6, 8, 10 m s^{-1}, from top to bottom, left to right). The water surface was covered by an OLA slick. Dashed line: wind only, solid line: rain and wind

The Doppler spectra measured at HV-polarisation at a rain rate of 160 mm h^{-1} (solid curves in Figure 6) are very similar in the whole wind-speed range used in the present investigation: they show a symmetric, broad peak with its maximum at about -40 dB. The location of this maximum, however, depends on wind speed because of the wind-induced surface drift. From this finding we conclude that the radar backscattering at cross-polarisation from a slick-covered water surface agitated by rain is

solely caused by rain-induced effects up to wind speeds of 8 m s^{-1}. As already pointed out by Braun et al. (2002) these effects may comprise stalks and cavities, or secondary drops.

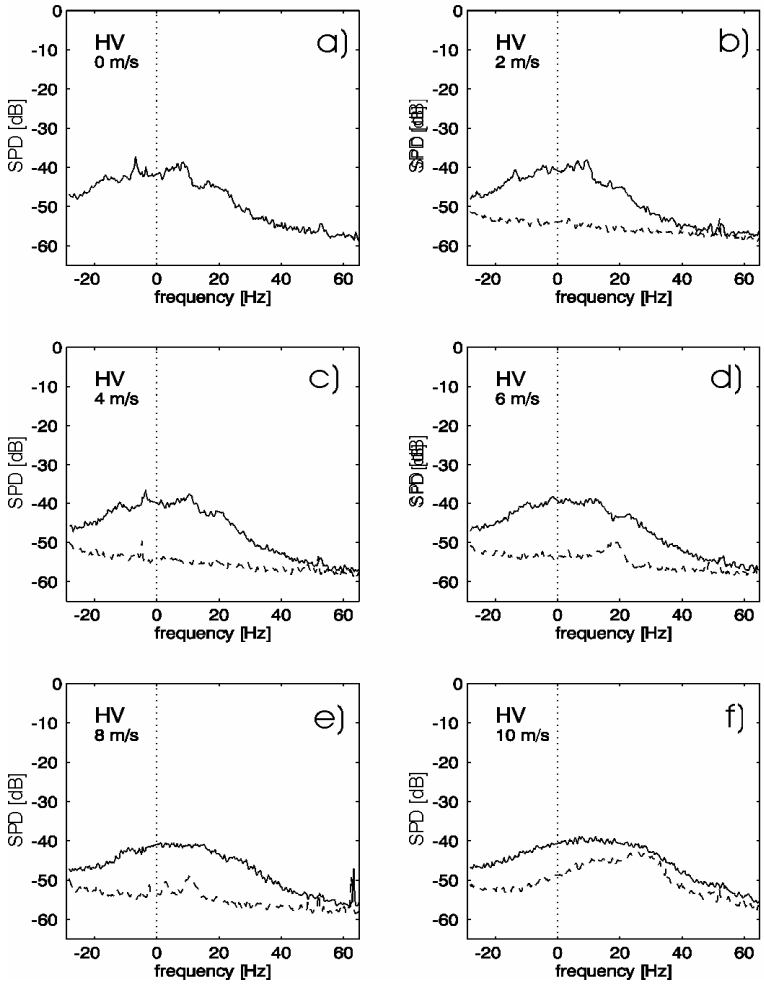

Fig. 6. Same as Figure 5, but for cross polarisation (HV)

Finally, the wind-dependence of the backscattered radar power (σ_{rel}) has been studied under different conditions. The results are shown in Figure 7, where the stars denote σ_{rel} values measured at a slick-free water surface and with rain, the circles denote σ_{rel} values measured at a slick-covered water surface and with rain, the crosses denote σ_{rel} values measured at a slick-

free water surface without rain, and the pluses denote σ_{rel} values measured at a slick-covered water surface without rain.

The upper diagram shows the measured σ_{rel} values for VV-polarisation, and the lower diagram shows the measured σ_{rel} values for cross-polarisation. It is obvious that the agitation of strong rain caused similar radar backscattering, independently of the slick coverage (see the stars and circles in Figure 7). That is, at high rain rates (like used in the present investigation) the enhancement of the radar backscattering by rain-induced effects such as ring waves, stalks, and cavities is not affected appreciably by the presence of a slick. This explains why the bright signature in the right panel of Figure 1 (X-band) is obviously not affected by the mineral oil spill.

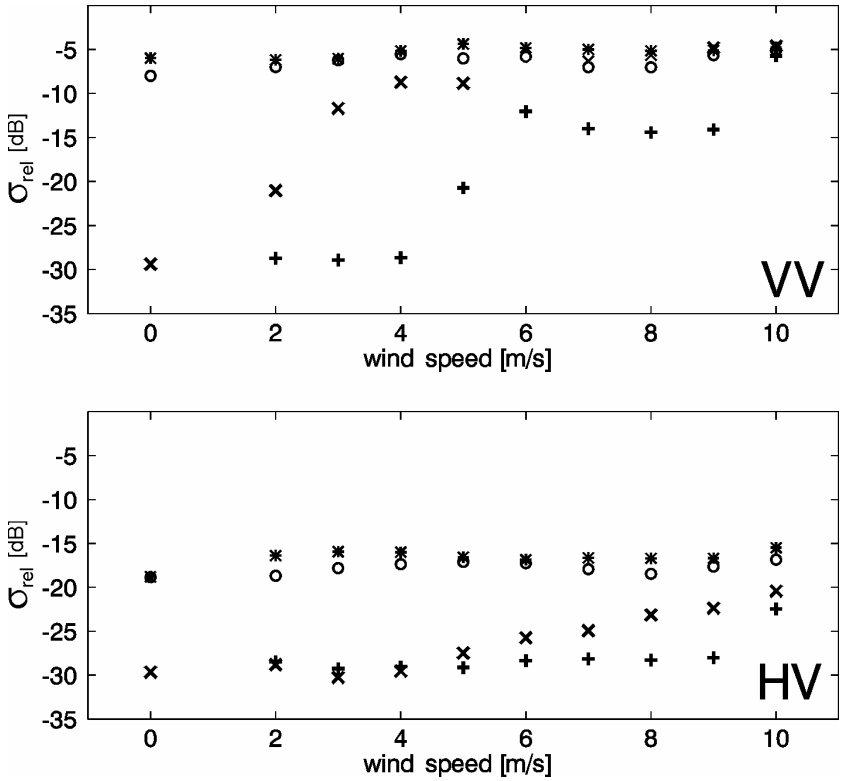

Fig. 7. Wind dependence of the relative backscattered radar power, σ_{rel}, measured under different conditions (×: slick-free, no rain; +: slick-covered, no rain; *: slick-free, with rain; o: slick-covered, with rain). Upper diagram: VV-polarization, lower diagram: HV-polarisation

The σ_{rel} values measured without rain (crosses and pluses in Figure 7, corresponding to a slick-free and to a slick-covered water surface, respectively) show that the reduction of the radar backscattering by monomolecular slicks is lower at cross-polarisation than at co-polarisation. This finding is in contrast to the results presented by Braun et al. (2002) and we suspect that this is due to an insufficient signal-to-noise ratio encountered during the herein presented measurements.

4 Summary and Conclusions

We have presented results of our laboratory measurements with artificial rain impinging on slick-free and slick-covered water surfaces. They show that the rain-induced roughness is not appreciably affected by slicks, whereas wind waves are strongly damped.

We have studied the dependence of the wave orientation ratio (measured with the two-dimensional laser slope gauge) on slick coverage and on wind speed. It can be inferred from our results that, on a slick-covered water surface, the rain-induced effects have an influence on the orientation of the wave field, particularly on the high-frequency part (up to 25 Hz), which is expected to be due to high frequency ring waves generated by the rain.

We also observed that, at wind speeds up to 8 m s^{-1}, the radar backscattering at co- and cross-polarisation is mainly caused by the rain-induced effects. Since similar results were obtained at slick-free water surfaces, we conclude that the coverage of the water surface by a monomolecular slick has no significant influence on the measured radar backscatter. However, we expect larger differences are to be found at lower rain rates.

Though our experiments were performed in a wind wave tank, where volume scattering at rain drops is negligible (cf. Melsheimer et al. 1998), our results may be transformed to lower radar frequencies. The splash products may strongly affect the radar backscattering at C-band, but volume scattering occurs only at very high rain rates. Therefore, our results are important for the interpretation of SAR images acquired by spaceborne SAR sensors at C-band (e.g., by those flown on the ERS, Envisat, and Radarsat satellites). That is, our results are suitable for the explanation of radar signatures of rain cells over the ocean, when its surface is covered by slicks or by mineral oil spills. However, in order to allow better knowledge of the influence of oceanic surface films on the imaging of strong rain events (and *vice versa*) additional experiments, particularly with lower rain rates and at different radar frequencies, are proposed.

5 References

Bliven LF, Sobieski PW, Craeye C (1997) Rain-generated ring waves: measurements and modelling for remote sensing. Int J Remote Sensing 18: 221–228

Braun N (1998) Laboruntersuchungen zum Einfluß von künstlichem Regen auf eine Wasseroberfläche mit Hilfe von Wellendraht-, Laser-, und Radarsonden. Diplomarbeit, Universität Hamburg, 99 pp

Braun N, Gade M, Lange PA (2002) The effect of artificial rain on wave spectra and multi-polarisation X band radar backscatter. Int J Remote Sensing 23: 4305-4322

Gade M, Alpers W, Ermakov SA, Hühnerfuss H, Lange PA (1998) Laboratory measurements of bound and freely propagating small gravity-capillary waves. J Geophys Res 103: 21697-21710

Laws JO (1941) Measurement of the fall-velocity of water-drops and raindrops. Trans Am Geophys Union 24: 452–460

Melsheimer C, Alpers W, Gade M (1998) Investigation of multi-frequency/multi-polarization radar signatures of rain cells, derived from SIR-C/X-SAR data. J Geophys Res 103: 18867-18884